

LENSING OBSERVABLES: MASSLESS DYONIC vis-à-vis ELLIS WORMHOLE

R.F. Lukmanova^{1,a}, G.Y. Tuleganova^{1,b}, R.N. Izmailov^{1,c},
and
K.K. Nandi^{1,2,d}

¹Zel'dovich International Center for Astrophysics, Bashkir State Pedagogical University named after M.Akmullah, 3A, October Revolution Street, Ufa 450008, RB, Russia

²High Energy and Cosmic Ray Research Center, University of North Bengal, Siliguri 734 013, WB, India

^aE-mail: mira789@mail.ru
^bE-mail: gulira.tuleganova@yandex.ru
^cE-mail: izmailov.ramil@gmail.com
^dE-mail: kamalnandi1952@yahoo.co.in

Abstract

Stable massless wormholes are theoretically interesting in their own right as well as for astrophysical applications, especially as galactic halo objects. Therefore, the study of gravitational lensing observables for such objects is of importance, and we do here by applying the parametric post-Newtonian method of Keeton and Petters to massless dyonic charged wormholes of the Einstein-Maxwell-Dilaton field theory and to the massless Ellis wormhole of the Einstein minimally coupled scalar field theory. The paper exemplifies how the lensing signatures of two different solutions belonging to two different theories could be qualitatively similar from the *observational* point of view. Quantitative differences appear depending on the parameter values. Surprisingly, there appears an unexpected divergence in the correction to differential time delay, which seems to call for a review of its original derivation.

1. Introduction

Gravitational lensing today is an inevitable part of astrophysicists' toolkit for probing a number of interesting phenomena dealing from compact objects to cosmology with widely varying distance scales. Especially, the importance of studying lensing signatures in the weak field limit lies in its ability to probe large-scale structures as well as the nature of the lens (see, e.g., Ref [1]). The central role in the lensing is played by the deflection of light caused by the gravitating lens, assumed here to be static and spherically symmetric. Light deflection angles caused by several Morris-Thorne traversable wormholes [2-8] and other objects [9-12] have been studied in the strong and weak field limit.

Among them, massless wormholes are stable [13-15] and have received particular attention [16]. By "massless", we mean that only the Keplerian mass is zero, while the energies of other nonvanishing fields go into making what is called the "Wheelerian mass" [17] that curves the space and it is this curvature that is revealed by light deflection. The weak field light deflection angle has been recently calculated in the literature by applying the Gauss-Bonnet Theorem (GBT) [18-22] to a class of massless dyonic wormholes, re-interpreted also as the Einstein-Rosen bridge.

Studying lensing signatures is a step farther than calculating merely the deflection angle since the signatures take us into the realm of expected observables. The motive of the present paper is to examine how these observables differ for different massless lenses. For an important application of lensing by the massless Ellis wormhole¹, which is a solution of Einstein minimally coupled scalar (EMS) field theory, it was shown by Abe [25] (this work was extended in Ref.[26]) that the weak field hypothesis is a good approximation for lensing by our galaxy if the throat radius is less than 10^{11} km. He further argued that if the massless wormholes, treated as Galactic halo objects, are bound to the Galaxy with throat radii between certain limits having a number density approximately equalling that of ordinary stars, then their detection is possible by analyzing the past data. Magnification of apparent brightness of distant stars lensed by an intermediate wormhole is another important lensing effect. In view of these astrophysically detectable effects and assuming that the halo region of galaxies are populated by massless Ellis wormholes as conjectured by Abe [25], it is of importance to calculate their observable signatures.

In this paper, we shall study the observables for massless dyonic wormhole in the Einstein-Maxwell-dilaton (EMD) theory [27] vis-à-vis those of massless Ellis wormhole of the EMS theory [23]. To that end, we shall first derive, using the Keeton-Petters (KP) method [28-30], the weak field deflection and lensing observables such as image positions, magnifications, centroid of a class of spherically symmetric static massless dyonic wormholes in the EMD theory that is already receiving attention (see, e.g., Ref. [16]). Next, we shall calculate the same observables associated with the massless Ellis wormhole in the EMS theory characterized by a scalar charge and tabulate a comparison between the wormholes. All observables will be expressed as a function of source angular position β . We shall graphically present quantitative differences in lensing observables for the two wormholes and point out an unexpected divergence in the correction to differential time delay.

The paper is section wise organized as follows. In Sec.II, we shall use the KP method to verify the expression for the weak field deflection angle by dyonic wormhole calculated by Jusufi *et al* [16]. In Sec.III, we shall calculate the lensing observables for the two massless wormholes under consideration. Sec.IV summarizes the paper.

¹To do justice, it should be called "Ellis-Bronnikov" wormhole since the two authors Ellis [23] and Bronnikov [24] discovered the solution independently and almost simultaneously in 1973. Nonetheless, we continue to call it Ellis wormhole here in order to avoid confusion with the prevailing nomenclature in the literature.

II. Weak field deflection angle by KP method

Keeton and Petters [29] developed a very useful framework for computing corrections to a core set of observable properties in a general asymptotically flat metric theory of gravity. The focus is to demonstrate how to handle lensing in competing gravity theories using post-post-Newtonian (PPN) correction terms up to third-order. Their method provides computation of *observable* quantities that are essentially coordinate independent and therefore are physically relevant. The readers are urged to consult the original series of papers by the authors [29].

The relevant EMD action is²

$$S_{\text{EMD}} = \int d^4x \sqrt{-g} \left[R - 2\partial_\mu \phi \partial^\mu \phi - e^{-2\phi} F_{\mu\nu} F^{\mu\nu} \right], \quad F_{\mu\nu} = \partial_\mu A_\nu - \partial_\nu A_\mu. \quad (1)$$

The dyonic massless wormhole in the (t, r, θ, φ) coordinates derived by Goulart [27] and subsequently studied by Jusufi *et al.* [16] is

$$d\tau^2 = -\frac{1}{1 + \frac{a^2}{r^2}} dt^2 + \frac{1 + \frac{a^2}{r^2}}{1 + \frac{k^2}{r^2}} dr^2 + (r^2 + a^2) (d\theta^2 + \sin^2 \theta d\varphi^2), \quad (2)$$

$$a^2 = 2PQ, \quad k^2 = \Sigma^2 + a^2, \quad F_{rt} = Q/r^2, \quad F_{\theta\varphi} = P \sin \theta, \quad (3)$$

$$e^{2\phi} = e^{2\phi_0} \frac{r + d_1}{r + d_0}, \quad d_1 = -d_0 = -\Sigma. \quad (4)$$

The solution represents a three-parameter wormhole characterized by electric charge (Q), magnetic charge (P) and a dilatonic charge (Σ). For the special case $\Sigma = 0$, this solution exactly coincides with the Einstein-Rosen bridge [22]. To apply the KP method, we express the metric (2) in isotropic coordinates (t, R, θ, φ) by introducing the transformation

$$r = \frac{R^2 - k^2}{2R}, \quad (5)$$

which when inverted yields $R = \frac{1}{2}r \left(1 \pm \sqrt{1 + k^2/r^2} \right)$. Discarding the negative sign, we find $\frac{R}{r} \rightarrow 1$ as $r \rightarrow \infty$, so at large distances R and r coincide. The metric (2) under the radial transformation (5) becomes

$$\begin{aligned} d\tau^2 &= -A(R)dt^2 + B(R) (dR^2 + R^2 d\theta^2 + R^2 \sin^2 \theta d\varphi^2) \\ &= -\left[\frac{1}{1 + \frac{4R^2 a^2}{(R^2 - k^2)^2}} \right] dt^2 \\ &\quad + \left[\frac{k^4 + 4a^2 R^2 - 2k^2 R^2 + R^4}{4R^4} \right] (dR^2 + R^2 d\theta^2 + R^2 \sin^2 \theta d\varphi^2). \end{aligned} \quad (6)$$

²Recently, Goulart [31] also derived phantom wormholes for a "sign reversed" kinetic term $+2\partial_\mu \phi \partial^\mu \phi$ in the EMD action (1), but we are considering only dyonic wormholes here.

This is an asymptotically flat metric, which is invariant under inversion: $R \rightarrow \frac{k^2}{R}$. The metric (2) thus represents a twice asymptotically flat regular wormhole as the spacetimes on either side of the throat appearing at $r_{\text{th}} = a = \sqrt{2PQ}$ (minimum areal radius) or at the isotropic radius $R_{\text{th}} = \frac{1}{2}a \left(1 + \sqrt{1 + k^2/a^2}\right)$ are regular. The tidal forces can also be verified to be finite everywhere. Now redefine $R = 2\bar{R}$ so that

$$d\tau^2 = -A(\bar{R})dt^2 + B(\bar{R}) \left(d\bar{R}^2 + \bar{R}^2 d\theta^2 + \bar{R}^2 \sin^2 \theta d\varphi^2 \right) \quad (7)$$

and the metric functions expand as

$$A(\bar{R}) = 1 - \frac{a^2}{\bar{R}^2} - \frac{a^4}{\bar{R}^4} \left(\frac{k^2}{2a^2} \right) + \dots \quad (8)$$

$$B(\bar{R}) = 1 + \frac{a^2}{\bar{R}^2} \left(1 - \frac{k^2}{2a^2} \right) + \frac{a^4}{\bar{R}^4} \left(\frac{k^4}{16a^4} \right) + \dots \quad (9)$$

Following the method of Keeton and Petters [29], and taking the PPN potential to be³

$$\frac{\Phi}{c^2} = \frac{a}{\bar{R}}, \quad (10)$$

we can have a PPN expansion as

$$A(\bar{R}) = 1 + 2\alpha' \left(\frac{\Phi}{c^2} \right) + 2\beta' \left(\frac{\Phi}{c^2} \right)^2 + \frac{3}{2}\xi' \left(\frac{\Phi}{c^2} \right)^3 + \dots \quad (11)$$

$$B(\bar{R}) = 1 - 2\gamma' \left(\frac{\Phi}{c^2} \right) + \frac{3}{2}\delta' \left(\frac{\Phi}{c^2} \right)^2 - \frac{1}{2}\eta' \left(\frac{\Phi}{c^2} \right)^3 + \dots \quad (12)$$

Since the KP method is relatively new, from here on, we outline the steps connecting the above coefficients α', β', γ' etc., for the isotropic form to the new coefficients $a_1, b_1, a_2, b_2, a_3, b_3$ for the standard form and then to the final coefficients A_1, A_2, A_3 . The latter coefficients all relate to the PPN expansion of the metric (7) written in the *standard* coordinates $(t, \rho, \theta, \varphi)$ in the form (in general, coordinate choices do not change physics, but in the standard coordinate system the surface area of a sphere is given by the familiar expression $4\pi\rho^2$)

$$d\tau^2 = -f(\rho)dt^2 + g(\rho)d\rho^2 + \rho^2 (d\theta^2 + \sin^2 \theta d\varphi^2), \quad (13)$$

where

$$f(\rho) = A(\bar{R}), g(\rho)d\rho^2 = B(\bar{R})d\bar{R}^2, \rho^2 = B(\bar{R})\bar{R}^2 \quad (14)$$

and the corresponding potential will be $\left(\frac{a}{\rho}\right)$. These transformations determine $f(\rho)$, $g(\rho)$ and connect the coefficients as desired. The next step is to note that the impact parameter b is related to the closest approach distance ρ_0 by

$$\frac{1}{b^2} = \frac{f(\rho_0)}{\rho_0^2}, \quad (15)$$

³Here a is the so-called "Wheelerian mass" made of the electric and magnetic field energies, while the dilaton Σ does not manifestly contribute to the potential.

which allows one to obtain

$$\rho_0 = b \left[1 - a_1 \left(\frac{a}{b} \right) + \frac{2a_2 - 3a_1^2}{2} \left(\frac{a}{b} \right)^2 + \dots \right]. \quad (16)$$

The final step is to expand the integrand in the exact deflection angle [34]

$$\hat{\alpha}(\rho_0) = 2 \int_{\rho_0}^{\infty} \frac{1}{\rho^2} \sqrt{\frac{f(\rho)g(\rho)}{1/b^2 - f(\rho)/\rho^2}} d\rho - \pi$$

in terms of the small PPN parameter $h = \frac{a}{\rho_0}$, integrate term by term, express ρ_0 in terms of b , which would immediately yield the coefficients A_1, A_2, A_3 of (22)-(24). By comparing similar powers between (8), (11) and between (9), (12), one finds

$$a_1 = \alpha' = 0, b_1 = \gamma' = 0, a_2 = \beta' - \alpha'\gamma' = -\frac{1}{2}, \quad (17)$$

$$b_2 = \frac{3\delta' + \gamma'^2}{4} = \frac{1}{2} \left(1 - \frac{k^2}{2a^2} \right), \xi' = 0, \eta' = 0, \quad (18)$$

$$a_3 = \frac{3\xi' + 3\alpha'\delta' - 8\beta'\gamma' + 2\alpha'\gamma'^2}{4} = 0, \quad (19)$$

$$b_3 = \frac{3\eta' + 15\delta'\gamma' - 2\gamma'^3}{16} = 0, \quad (20)$$

The two way deflection angle is

$$\hat{\alpha}(b) = A_1 \left(\frac{a}{b} \right) + A_2 \left(\frac{a}{b} \right)^2 + A_3 \left(\frac{a}{b} \right)^3 + \dots \quad (21)$$

where b is the invariant impact parameter related to the closest approach distance r_0 to leading order by $b = r_0 \left(1 + a_1 \frac{a}{R} \right) = r_0$. Also

$$A_1 = 2(a_1 + b_1), \quad (22)$$

$$A_2 = \left(2a_1^2 - a_2 + a_1b_1 - \frac{b_1^2}{4} + b_2 \right) \pi, \quad (23)$$

$$A_3 = \frac{2}{3} [35a_1^3 + 15a_1^2b_1 - 3a_1(10a_2 + b_1^2 - 4b_2) + 6a_3 + b_1^3 - 6a_2b_1 - 4b_1b_2 + 8b_3]. \quad (24)$$

In view of the values in (17)-(20), we find

$$A_1 = 0, A_2 = \left(1 - \frac{a^2 + \Sigma^2}{4a^2} \right) \pi, A_3 = 0, \quad (25)$$

so the invariant deflection angle is

$$\hat{\alpha}(b) = A_2 \left(\frac{a}{b} \right)^2 = \frac{3\pi PQ}{2b^2} - \frac{\pi\Sigma^2}{4b^2}. \quad (26)$$

This result exactly agrees with the deflection angle obtained by Jusufi *et al.* [16], who used the GBT method. This agreement suggests that the potential $\frac{\Phi}{c^2} = \frac{a}{R}$ is the correct one, which does not contain the dilatonic charge Σ , although interestingly it does contribute to the deflection angle and the actual lensing observables. Incidentally, since $A_3 = 0$, the third order term $(\frac{a}{b})^3$ is *absent* in the deflection. This non-trivial information about the weak field deflection is difficult to obtain by GBT method but here it is easily obtained from the Keeton-Petters method.

The weak field deflection $\hat{\alpha}$ in general has a major difference with strong field deflection. The strong field deflection suffered by light rays passing at an invariant impact parameter b closest to the photon sphere have a logarithmic divergence [32,33]. This fact prevents the *exact* deflection angle to be Taylor expanded to yield the same light deflection for the same b . For instance [33], for the Schwarzschild black hole of mass M ,

$$\hat{\alpha}_{\text{strong}}(b') = -\pi + \log \left[\frac{216(7 - 4\sqrt{3})}{b'} \right] + O(b'), \quad (27)$$

$$\hat{\alpha}_{\text{weak}}(b') = \frac{4}{3\sqrt{3}} (1 - b') + O(1 - b')^2, \quad (28)$$

where the redefined common impact parameter b' is $1 - b' = \frac{3\sqrt{3}M}{b}$. When $b = 3\sqrt{3}M$, $\hat{\alpha}_{\text{strong}} \rightarrow \infty$, but $\hat{\alpha}_{\text{weak}} = \frac{4M}{b}$, as expected. These facts indicate that the weak field lensing is expected to yield a set of lensing observables completely different from those of the strong field. We note that $\hat{\alpha}_{\text{strong}}$ is itself an approximation in the strong regime with $O(b')$ neglected.⁴

III. Lensing observables

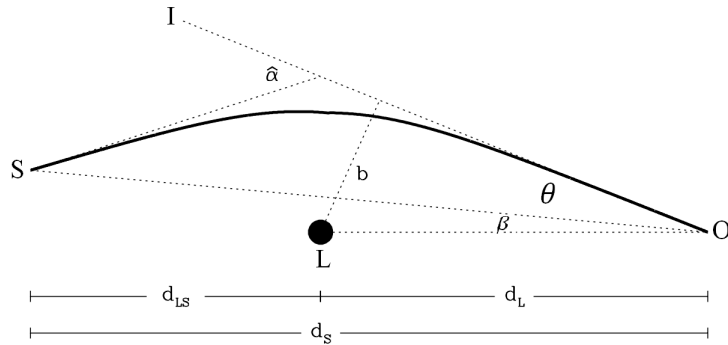


Figure 1: Lens geometry.

⁴We thank an anonymous referee for pointing it out.

The lens geometry is shown in Fig.1. The corresponding lens equation, with the angles scaled by the Einstein angle θ_E , is [35]

$$\tan \beta = \tan \theta - D [\tan \theta + \tan(\hat{\alpha} - \theta)], \quad (29)$$

where $\hat{\alpha}$ is the light deflection angle, β is the source angular position, θ is the angular position of the image and $D \equiv d_{LS}/d_S$. This equation, though obtained from elementary trigonometry of Fig.1, very well describes the full relativistic treatment for light propagation. The next step is to expand the angular position θ of the image as

$$\theta = \theta_0 + \theta_1 \varepsilon + \theta_2 \varepsilon^2 + O(\varepsilon^3), \quad (30)$$

where θ_0 represents the image position in the weak deflection limit, while θ_1, θ_2 represent first- and second-order correction terms, θ_E is the Einstein angle, ε is the small perturbative parameter defined by

$$\varepsilon \equiv \frac{\theta_E}{4D}, \quad \theta_E \equiv \sqrt{\frac{4Gad_{LS}}{c^2 d_L d_S}}. \quad (31)$$

Using the expansion for θ , the exact bending angle can be expanded as [31] (terms in ε^3 not shown, to save space)

$$\hat{\alpha} = \frac{A_1}{\theta_0} \varepsilon + \frac{A_2 - A_1 \theta_1}{\theta_0^2} \varepsilon^2 + \dots \quad (32)$$

Substituting θ and $\hat{\alpha}$ in the lens equation and expanding it beyond linear order, one has

$$0 = D \left[-4\beta + 4\theta_0 - \frac{A_1}{\theta_0} \right] \varepsilon + \frac{D}{\theta_0^2} [-A_2 + (A_1 + 4\theta_0^2) \theta_1] \varepsilon^2 + \dots \quad (33)$$

The lensing observables are obtained as follows. Note that each coefficient in the expression (33) should vanish since ε can be independently varied, which then yields the first observable, the *image position* θ_0 and correction θ_1 to it (the expression for θ_2 not shown)

$$\theta_0 = \frac{1}{2} \left[\sqrt{A_1 + \beta^2} + \beta \right], \quad \theta_1 = \frac{A_2}{A_1 + 4\theta_0^2}. \quad (34)$$

Magnification $\mu(\theta)$ of images takes place because the bending of light by the lens focusses more light rays from the source into a solid angle at the observer brightening up the image. It is defined by

$$\mu(\theta) = \left[\frac{\sin \beta}{\sin \theta} \frac{d\beta}{d\theta} \right]^{-1}. \quad (35)$$

Exactly the same procedure as for the image position and correction applies to this case too. By using the expressions for θ_1, θ_2 , one can write a series expansion as

$$\mu = \mu_0 + \mu_1 \varepsilon + \mu_2 \varepsilon^2 + O(\varepsilon)^3, \quad (36)$$

which yields magnification μ_0 and its correction μ_1 (μ_2 not shown)

$$\mu_0 = \frac{16\theta_0^4}{16\theta_0^4 - A_1^2}, \quad \mu_1 = \frac{16A_2\theta_0^3}{(A_1 + 4\theta_0^2)^3}. \quad (37)$$

In the case when the individual images are too close together and cannot be resolved, it is useful to define *total magnification* μ_{tot} as a sum of magnification of positive and negative parity images μ^+ and μ^- as

$$\begin{aligned} \mu_{\text{tot}} &= |\mu^+| + |\mu^-| \\ &= \frac{16A_1^2(\theta_0^8 - 1)}{(16\theta_0^4 - A_1^2)(A_1^2\theta_0^2 - 16)} \\ &\quad - \frac{16(A_1 - 4)A_2\theta_0^3}{(A_1 + 4\theta_0^2)^3(4 + A_1\theta_0^2)^3} \{[16 + A_1(4 + A_1)] \\ &\quad \times (\theta_0^6 - 1) + 12A_1\theta_0^2(\theta_0^2 - 1)\} \varepsilon + O(\varepsilon)^2. \end{aligned} \quad (38)$$

The center of light or in short the *centroid* Θ_{cent} of the images is simply the magnification-weighted sum of the image positions and its expansion is

$$\Theta_{\text{cent}} = \Theta_{\text{cent},0} + \Theta_{\text{cent},1}\varepsilon + \Theta_{\text{cent},2}\varepsilon^2 + O(\varepsilon)^3 \quad (39)$$

$$\Theta_{\text{cent},0} = |\beta| \frac{3A_1 + 4\beta^2}{2A_1 + 4\beta^2}, \quad \Theta_{\text{cent},1} = 0, \quad (40)$$

where $\Theta_{\text{cent},2}$ is not shown.

The *differential time delay* $\Delta\hat{\tau}$ is the delay in the arrival times at the observer from a pair of images and is also PPN expanded in terms of ε (see below).

(A) Dyonic massless wormhole

The PPN parameters in standard coordinates in this case are

$$a_1 = a_3 = b_1 = b_3 = 0, \quad a_2 = -\frac{1}{2}, \quad b_2 = \frac{1}{2} - \frac{k^2}{4a^2}, \quad (41)$$

$$A_1 = 0, \quad A_2 = \pi \left(1 - \frac{k^2}{4a^2}\right), \quad A_3 = 0. \quad (42)$$

The lensing observables are as follows.

(i) Image position and corrections

$$\theta_0 = \beta, \quad \theta_1 = \frac{\pi}{4\beta^2} \left(1 - \frac{k^2}{4a^2}\right), \quad \theta_2 = -\frac{\pi^2}{8\beta^5} \left(1 - \frac{k^2}{4a^2}\right)^2. \quad (43)$$

(ii) Magnification and corrections

$$\mu_0 = 1, \quad \mu_1 = -\frac{\pi}{4\beta^3} \left(1 - \frac{k^2}{4a^2}\right), \quad \mu_2 = -\frac{3\pi^2}{8\beta^6} \left(1 - \frac{k^2}{4a^2}\right)^2. \quad (44)$$

(iii) Total magnification, centroid and corrections

$$\mu_{\text{tot}} = \frac{3\pi^2}{4\beta^6} \left(1 - \frac{k^2}{4a^2}\right) \varepsilon^2, \quad (45)$$

$$\Theta_{\text{cent},0} = |\beta|, \quad \Theta_{\text{cent},1} = 0, \quad \Theta_{\text{cent},2} = -\frac{3\pi^2}{8\beta^5} \left(1 - \frac{k^2}{4a^2}\right)^2. \quad (46)$$

(iv) Differential time delay and corrections

$$\Delta\hat{\tau} = \Delta\hat{\tau}_0 + \Delta\hat{\tau}_1 \varepsilon + O(\varepsilon)^2, \quad (47)$$

where

$$\Delta\hat{\tau}_0 = \frac{1}{2} |\beta| \sqrt{A_1 + \beta^2} + \frac{A_1}{4} \ln \left(\frac{\sqrt{A_1 + \beta^2} + \beta}{\sqrt{A_1 + \beta^2} - \beta} \right), \quad (48)$$

$$\Delta\hat{\tau}_1 = \frac{A_2}{A_1} |\beta|. \quad (49)$$

In the present case, since $A_1 = 0$, we find

$$\Delta\hat{\tau}_0 = \frac{\beta^2}{2}, \quad \Delta\hat{\tau}_1 \rightarrow \text{divergent}. \quad (50)$$

One way to interpret this divergence in the differential time delay correction is the following. If we set $A_2 = 0$, $\beta \neq 0$, then the correction $\Delta\hat{\tau}_1$ vanish and measurement of $\Delta\hat{\tau}_0$ would allow one to determine location of the angular position β of the source. When $A_2 \neq 0$, $\beta = 0$, the source, lens, and observer are aligned and in this case, one has an *Einstein ring* from where light reaches the observer exactly at the same time so that there is no time delay, hence, $\Delta\hat{\tau}_0 = 0$. Since there are no individual images now, the corrections attributable to individual images also lose their meaning, a symptom of which is the appearance of divergences in Eqs.(50).

(b) Ellis massless wormhole

The action is

$$S_{\text{EMS}} = \int d^4x \sqrt{-g} [R + 2\partial_\mu \Psi \partial^\mu \Psi], \quad (51)$$

where the kinetic term $+2\partial_\mu \Psi \partial^\mu \Psi$ is sign reversed here compared to that in action (1) meaning that the field Ψ represents exotic phantom matter. The Ellis massless solution is given by

$$d\tau^2 = -dt^2 + d\ell^2 + (\ell^2 + m^2) (d\theta^2 + \sin^2 \theta d\varphi^2), \quad (52)$$

$$\Psi = \frac{1}{\sqrt{2}} \left[\frac{\pi}{2} - 2 \tan^{-1} \left(\frac{\ell}{m} \right) \right], \quad (53)$$

where m is a constant of integration that can be called the scalar charge proportional to the integrated total energy of the scalar field Ψ . Under the transformation $\ell^2 + m^2 = \rho^2$, the metric reduces in standard coordinates $(t, \rho, \theta, \varphi)$

to the form

$$d\tau^2 = -dt^2 + \frac{d\rho^2}{1 - \frac{m^2}{\rho^2}} + \rho^2 (d\theta^2 + \sin^2 \theta d\varphi^2). \quad (54)$$

Taking the PPN potential $\frac{\psi}{c^2} = \frac{m}{\rho}$, we find the coefficients to be

$$a_1 = a_2 = a_3 = b_1 = b_3 = 0, \quad b_2 = \frac{1}{4}, \quad (55)$$

$$A_1 = 0, \quad A_2 = \frac{\pi}{4}, \quad A_3 = 0. \quad (56)$$

The bending angle then follows as

$$\hat{\alpha}_{\text{weak}}(b) = \frac{\pi m^2}{4b^2}, \quad (57)$$

which exactly reproduces the leading order term of the deflection calculated by Bhattacharya and Potapov [6] by three independent ways other than the KP method.

(i) Image position and corrections:

$$\theta_0 = \beta, \quad \theta_1 = \frac{\pi}{16\beta^2}, \quad \theta_2 = -\frac{\pi^2}{128\beta^5}. \quad (58)$$

(ii) Magnification and corrections:

$$\mu_0 = 1, \quad \mu_1 = -\frac{\pi}{16\beta^3}, \quad \mu_2 = -\frac{3\pi^2}{128\beta^6}. \quad (59)$$

(iii) Total magnification, centroid and corrections:

$$\mu_{\text{tot}} = \frac{3\pi^2 \varepsilon^2}{64\beta^6}, \quad (60)$$

$$\Theta_{\text{cent},0} = |\beta|, \quad \Theta_{\text{cent},1} = 0, \quad \Theta_{\text{cent},2} = -\frac{3\pi^2}{128\beta^5}. \quad (61)$$

(iv) Differential time delay and corrections:

The same expressions as in (48) and (49) apply, so that

$$\Delta\hat{\tau}_0 = \frac{\beta^2}{2}, \quad \Delta\hat{\tau}_1 \rightarrow \text{divergent}. \quad (62)$$

Same arguments about divergence following Eq.(50) apply here too and need not be repeated. The foregoing results are tabulated in Table 1 below for easy comparison.

TABLE I
PPN observables for dyonic and Ellis wormholes

Observable	Dyonic wormhole	Ellis wormhole
θ_0	β	β
θ_1	$\frac{\pi}{4\beta^2} \left(1 - \frac{k^2}{4a^2}\right)$	$\frac{\pi}{16\beta^2}$
θ_2	$-\frac{\pi^2}{8\beta^5} \left(1 - \frac{k^2}{4a^2}\right)^2$	$-\frac{\pi^2}{128\beta^5}$
μ_0	1	1
μ_1	$-\frac{\pi}{4\beta^3} \left(1 - \frac{k^2}{4a^2}\right)$	$-\frac{\pi}{16\beta^3}$
μ_2	$-\frac{3\pi^2}{8\beta^6} \left(1 - \frac{k^2}{4a^2}\right)^2$	$-\frac{3\pi^2}{128\beta^6}$
μ_{tot}	$\frac{3\pi^2}{4\beta^6} \left(1 - \frac{k^2}{4a^2}\right) \varepsilon^2$	$\frac{3\pi^2}{64\beta^6} \varepsilon^2$
$\Theta_{\text{cent},0}$	$ \beta $	$ \beta $
$\Theta_{\text{cent},1}$	0	0
$\Theta_{\text{cent},2}$	$-\frac{3\pi^2}{8\beta^5} \left(1 - \frac{k^2}{4a^2}\right)^2$	$-\frac{3\pi^2}{128\beta^5}$
$\Delta\hat{\tau}_0$	$\frac{\beta^2}{2}$	$\frac{\beta^2}{2}$
$\Delta\hat{\tau}_1$	divergent	divergent

4. Summary

The purpose of this paper was to investigate gravitational lensing signatures of massless asymptotically flat wormholes in the two theories described by the two actions (1) and (51). It is evident that the kinetic term has different signs indicating that the nature of the source matter is quite different in either action. The energy conditions are violated at the solution level necessary to make the two solutions wormholes. Further, the metrics do not coincide in an ordinary one-to-one correspondence of their parameters on a real line, and neither are they connected by any coordinate transformation. So the solutions are non-trivially different. It turns out that the Ellis metric (52) follows from the dyonic metric (2) only when $a = 0$, and $\Sigma^2 = -m^2$, meaning an *imaginary* dilatonic charge. It shows that the two metrics represent physically different wormholes. On the other hand, the dilaton Σ does not contribute to the central potential (10) though it does contribute to energy conditions and observables. The situation therefore is a very curious one deserving a closer scrutiny of the lensing behavior of the two objects, which we have done above.

We computed weak field lensing observables by applying the PPN method of Keeton and Petters (KP) to massless dyonic and Ellis wormholes. The paper nicely exemplifies how the observable lensing signatures of two physically different objects originating from very different parent theories could still be qualitatively similar from the *observational* point of view. Quantitative differences appear depending on the parameter values. Quantitative differences appear depending on the parameter values P , Q , Σ and on the source angular position β . In the special case $\Sigma = \sqrt{6PQ}$, where P and Q are magnetic and electric charge respectively, the observables between the two wormholes drastically differ - all the correction factors vanish for the dyonic charged wormhole, while they remain nonzero for the Ellis wormhole. The observables in the two cases are tabulated

for easy view. For illustrative purposes and numerical comparison, we take the black hole SgrA* residing at the center of our galaxy and treat it as a massless wormhole made by a high concentration of "Wheelerian mass" (made of P, Q or m). In that case, it follows that [27] $\varepsilon = 1.3 \times 10^{-4} \left(\frac{d_{LS}}{10 \text{ pc}} \right)^{-1/2}$, which is used for all the Figs.2-7.

We notice that the correction $\Delta\hat{\tau}_1$ to differential time delay from individual images surprisingly *diverge* in both the wormholes since $A_1 = 0$ despite the fact that all other observables are finite as tabulated. Such a divergence in the weak field is thus an unexpected behavior. Probably, it signals that the derivation of $\Delta\hat{\tau}_1$ needs to be reviewed. The divergence can be avoided only if $\beta = 0$, which means the source, lens and the observer are to be situated on a straight line and the image will be an Einstein ring instead of individual images. There would be no differential time delay in this case.

Acknowledment

The authors thank an anonymous referee for his/her useful suggestions that helped improve the paper. The reported study was funded by RFBR according to the research Project No. 18-32-00377.

References

- [1] A. Giahi-Saravani and B. M. Schäfer, Mon. Not. R. Astron. Soc. **437**, 2 (2014).
- [2] L. Chetouani and G. Clement, Gen. Rel. Grav. **16**, 111 (1984).
- [3] Y. Toki, T. Kitamura, H. Asada and F. Abe, Astrophys. J. **740**, 121 (2011).
- [4] V. Perlick, Phys. Rev. D **69**, 064017 (2004).
- [5] K. K. Nandi, Y.Z. Zhang and A. V. Zakharov, Phys. Rev. D **74**, 024020 (2006).
- [6] A. Bhattacharya and A.A. Potapov, Mod. Phys. Lett. A **25**, 2399 (2010).
- [7] K. K. Nandi, R. N. Izmailov, A. A. Yanbekov and A. A. Shayakhmetov, Phys. Rev. D **95**, 104011 (2017).
- [8] A. Tamang, A. A. Potapov, R. Lukmanova, R. Izmailov and K. K. Nandi, Class.Quant.Grav. **32**, 235028 (2015).
- [9] A. Bhadra, Phys. Rev. D **67**, 103009 (2003).
- [10] T. Harko and F. S. N. Lobo, Phys. Rev. D **92**, 043011 (2015).
- [11] A. Bhadra, K. Sarkar and K. K. Nandi, Phys. Rev. D **75**, 123004 (2007).
- [12] C. Cattani, M. Scalia, E. Laserra, I. Bochicchio and K.K. Nandi, Phys. Rev. D **87**, 047503 (2013).
- [13] C. Armendáriz-Pícon, Phys. Rev. D **65**, 104010 (2002).
- [14] K. K. Nandi, A. A. Potapov, R. N. Izmailov, A. Tamang and J. C. Evans, Phys. Rev. D **93**, 104044 (2016).
- [15] I. D. Novikov and A. A. Shatskiy, J. Exp. Theor. Phys. **114**, 801 (2012).
- [16] K. Jusufi, A. Övgün and A. Banerjee, Phys. Rev. D **96**, 084036 (2017).

- [17] M. Visser, Lorentzian Wormholes-From Einstein To Hawking (AIP, New York, 1995).
- [18] K. Jusufi, F. Rahaman and A. Banerjee, Ann. Phys. (Amsterdam) **389**, 219 (2018).
- [19] A. Ishihara, Y. Suzuki, T. Ono, T. Kitamura and H. Asada, Phys. Rev. D **94**, 084015 (2016).
- [20] H. Arakida, Gen. Relativ. Gravit. **50**, 48 (2018).
- [21] N. Tsukamoto, T. Kitamura, K. Nakajima and H. Asada, Phys. Rev. D **90**, 064043 (2014).
- [22] K. Jusufi, N. Sarkar, F. Rahaman, A. Banerjee and S. Hansraj, Eur.Phys. J. C **78**, 349 (2108).
- [23] H. G. Ellis, J. Math. Phys. **14**, 104 (1973); **15**, 520 (E) (1974).
- [24] K. A. Bronnikov, Acta Phys. Pol. B **4**, 251 (1973).
- [25] F. Abe, Astrophys. J. **725**, 787 (2010).
- [26] R. Lukmanova, A. Kulbakova, R. Izmailov and A. A. Potapov, Int. J. Theor. Phys. **55**, 4723 (2016).
- [27] P. Goulart, arXiv:1611.03093.
- [28] C. R. Keeton and A.O. Petters, Phys. Rev. D **72**, 104006 (2005).
- [29] C. R. Keeton and A. O. Petters, Phys.Rev. D **73**, 044024 (2006).
- [30] C. R. Keeton and A. O. Petters, Phys.Rev. D **73**, 104032 (2006).
- [31] P. Goulart, Class. Quantum Grav. **35**, 025012 (2018).
- [32] V. Bozza, Phys. Rev. D **66**, 103001 (2002).
- [33] S.V. Iyer and A.O. Petters, Gen. Rel. Grav. **39**, 1563 (2007).
- [34] K.S. Virbhadra, D. Narasimha and S.M. Chitre, Astron. Astrophys. **337**, 1–8 (1998).
- [35] K.S. Virbhadra and, G.F.R. Ellis, Phys. Rev. D **62**, 084003 (2000).

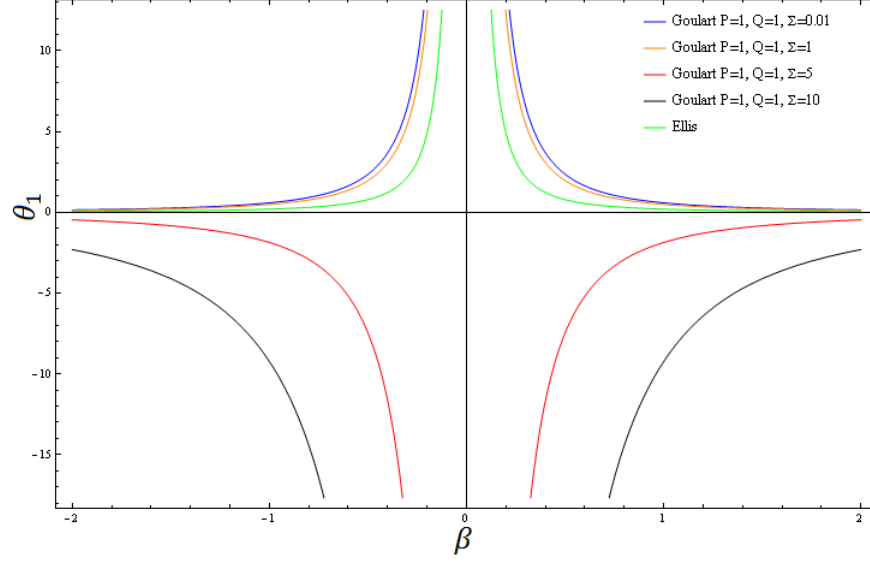


Figure 2: The second-order correction θ_1 for the source angular position $\beta \in [-2; 2]$.

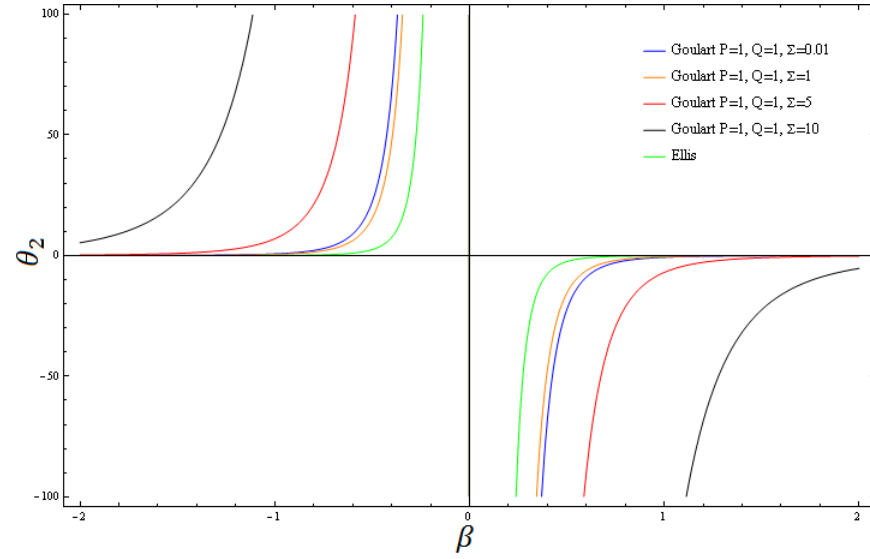


Figure 3: The second-order correction θ_2 for the source angular position $\beta \in [-2; 2]$.

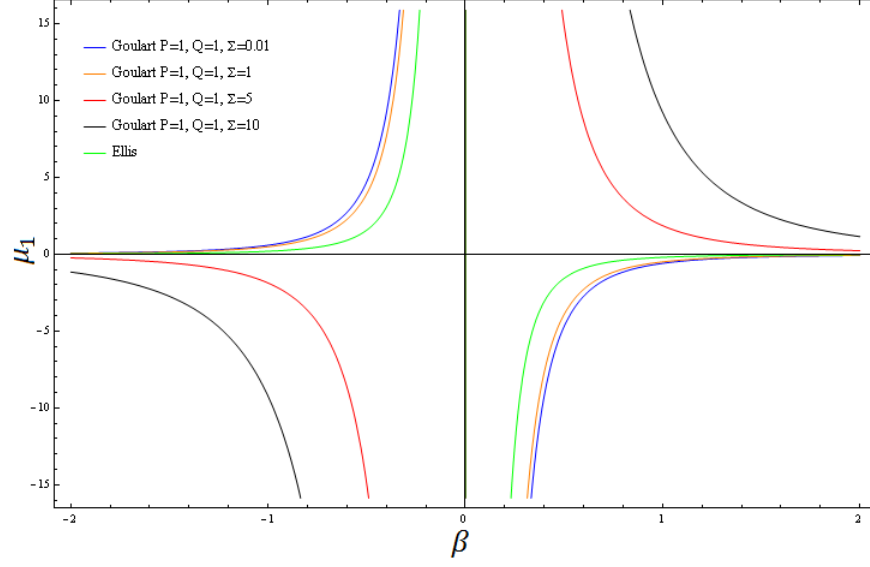


Figure 4: The first-order correction μ_1 for the source angular position $\beta \in [-2; 2]$.

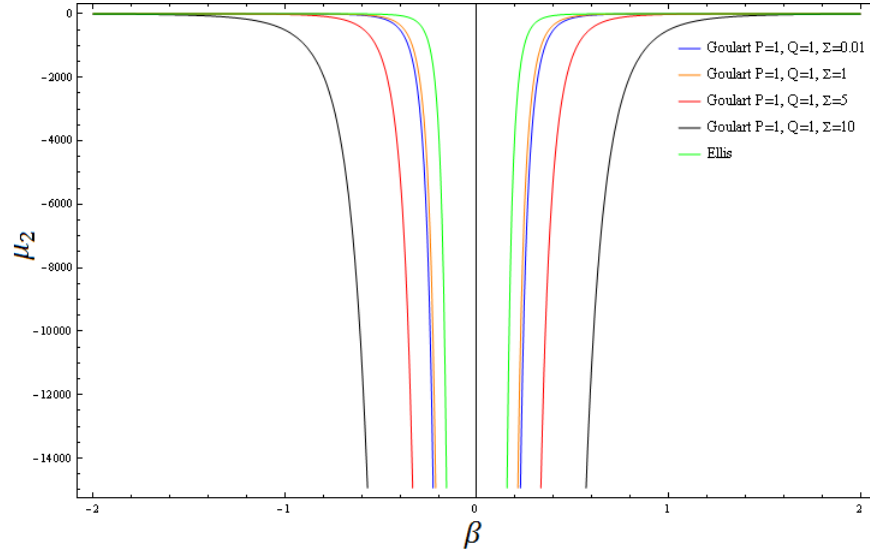


Figure 5: The second-order correction μ_2 for the source angular position $\beta \in [-2; 2]$.

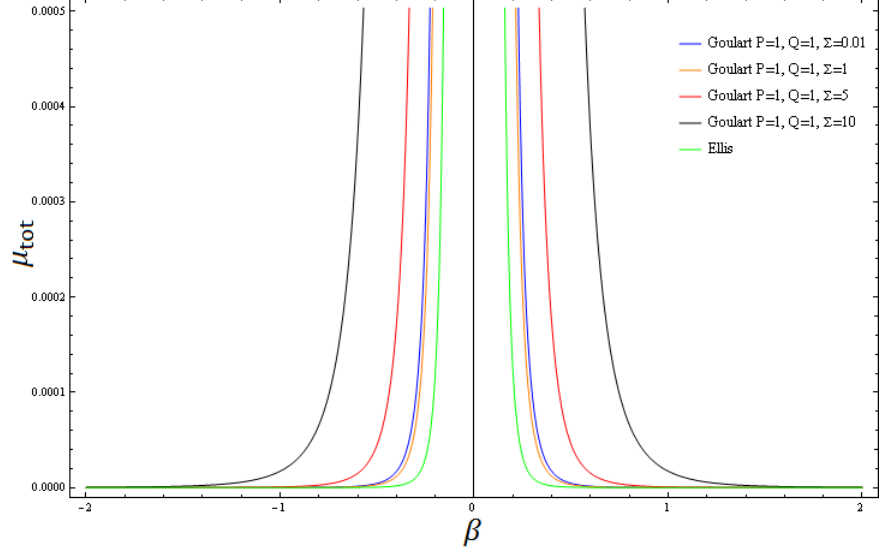


Figure 6: The total magnification μ_{tot} for the source angular position $\beta \in [-2; 2]$.

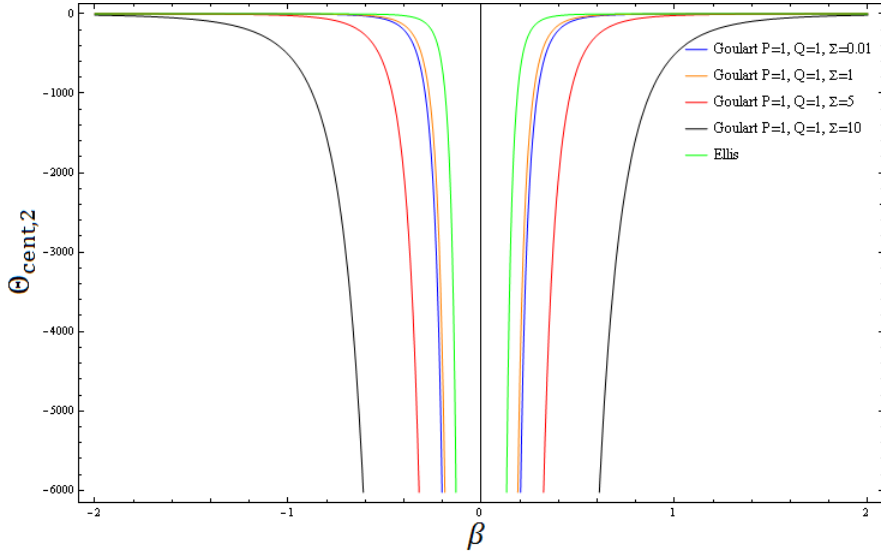


Figure 7: The second-order correction $\Theta_{\text{cent},2}$ for the source angular position $\beta \in [-2; 2]$.